Production cross section and decay study of ²⁴³Es and ²⁴⁹Md

R. Briselet,¹ Ch. Theisen,¹, ª M. Vandebrouck,¹ A. Marchix,¹ M. Airiau,¹ K. Auranen,²,ᵇ H. Badran,² F. Bisso,²

D. Boilley,³,⁴ T. Calverley,²,⁵ D. Cox,²,⁵,ᶜ F. Déchery,¹,⁶ A. Drouart,¹ B. Gall,⁶ T. Goigoux,¹ T. Grahn,²

P. T. Greenlees,² K. Hauschild,⁷ A. Herzan,²,ᵈ R. D. Herzberg,⁵ U. Jakobsson,²,ᵉ R. Julin,² S. Juutinen,²

J. Konki,²,ᶠ M. Leino,² A. Lightfoot,² A. Lopez-Martens,⁷ A. Mistry,⁵,ᵍ P. Nieminen,²,ʰ J. Pakarinen,²

P. Papadakis,²,⁵ J. Partanen,² P. Peura,² P. Rahkila,² J. Rubert,⁶ P. Ruotsalainen,² M. Sandzelius,²

J. Saren,² C. Scholey,² J. Sorri,²,ⁱ S. Stolze,²,ᵇ B. Sulignano,¹ J. Uusitalo,² A. Ward,⁵ and M. Zielińska¹

¹*Irfu, CEA, Université Paris-Saclay, F-91191 Gif-sur-Yvette, France*
²*University of Jyvaskyla, Department of Physics, P.O. Box 35, FI-40014 Jyvaskyla, Finland*
³*GANIL, CEA/DRF-CNRS/IN2P3, BP 55027, F-14076 Caen cedex 5, France*
⁴*Normandie Université, UNICAEN, Caen, France*
⁵*University of Liverpool, Department of Physics,*
Oliver Lodge Laboratory, Liverpool L69 7ZE, UK
⁶*Institut Pluridisciplinaire Hubert Curien, F-67037 Strasbourg, France*
⁷*CSNSM, IN2P3-CNRS, F-91405 Orsay Campus, France*
(Dated: September 28, 2018)

In the study of the odd-Z, even-N nuclei ²⁴³Es and ²⁴⁹Md, performed at the University of Jyväskylä, the fusion-evaporation reactions ¹⁹⁷Au(⁴⁸Ca,2n)²⁴³Es and ²⁰³Tl(⁴⁸Ca,2n)²⁴⁹Md have been used for the first time. Fusion-evaporation residues were selected and detected using the RITU gas-filled separator coupled with the focal-plane spectrometer GREAT. For ²⁴³Es, the recoil decay correlation analysis yielded a half-life of 24 ± 3 s, and a maximum production cross section of 37 ± 10 nb. In the same way, a half-life of 26 ± 1 s, a α branching ratio of $75 \pm 5\%$, and a maximum production cross section of 300 ± 80 nb were determined for ²⁴⁹Md. The decay properties of ²⁴⁵Es, the daughter of ²⁴⁹Md, were also measured: a α branching ratio of $54 \pm 7\%$ and a half-life of 65 ± 6 s. Experimental cross sections were compared to the results of calculations performed using the KEWPIE2 statistical fusion-evaporation code.

I. INTRODUCTION

Determining the boundaries of the nuclear chart, particularly in the region of super-heavy nuclei (SHN), is one of the key questions driving fundamental nuclear physics. The SHN owe their existence to shell effects, as without them the Coulomb repulsion would make the nuclei beyond $Z = 104$ unstable against fission [1]. In this context, detailed spectroscopy of very heavy nuclei (VHN) and SHN is of paramount importance to provide information on the nuclear landscape close to the high-A limit of the nuclear chart, as well as on the nature of the predicted island of stability. The challenge of these experiments is related to low production cross sections and, in odd-

mass nuclei, to the complexity of spectra where various collective and single-particle excitations may lie close in energy. On the other hand, the studies of odd-mass nuclei are rewarded by the wealth of information regarding single-particle states, exceeding what can be obtained for even-even nuclei [2].

Regarding the known excited states of single-particle or collective nature, little data is available for Es ($Z = 99$) and Md ($Z = 101$) isotopes [2, 3]. Before in-beam spectroscopy of these odd-Z nuclei can be attempted, feasibility studies are a prerequisite, in particular measurements of production cross sections. Such measurements also help to improve the description of the fusion-evaporation reaction mechanism, providing new constraints for the models.

In this paper, the production cross sections for ²⁴³Es and ²⁴⁹Md populated directly in the fusion-evaporation reactions ¹⁹⁷Au(⁴⁸Ca,2n)²⁴³Es and ²⁰³Tl(⁴⁸Ca,2n)²⁴⁹Md are reported. The targets and projectiles were chosen as a compromise between the predicted production cross sections and the transmission in the separator. In particular, very asymmetric reactions using actinide targets were not considered, as in such cases (i) the large angular dispersion due to the low recoil velocity and neutron emission results in a poor transmission, (ii) the low recoil energy reduces the detection efficiency at the focal plane, both effects being not fully compensated by enhanced cross sections.

The present study also allowed the half-lives and decay properties of these nuclei to be updated, as well as those

ª E-mail: christophe.theisen@cea.fr
ᵇ Present address: Physics Division, Argonne National Laboratory, 9700 South Cass Avenue, Lemont, Illinois 60439, USA
ᶜ Present address: University of Lund, Box 118, 221 00 Lund, Sweden
ᵈ Present Address: Institute of Physics, Slovak Academy of Sciences, SK-84511 Bratislava, Slovakia
ᵉ Present Address: Laboratory of Radiochemistry, Department of Chemistry, P.O. Box 55, FI-00014 University of Helsinki, Finland
ᶠ Present address: CERN, CH-1211 Geneva 23, Switzerland
ᵍ Present address: GSI Helmholtzzentrum für Schwerionenforschung GmbH, 64291 Darmstadt, Germany
ʰ Present Address: Fortum Oyj, Power Division, P.O. Box 100, 00048 Fortum, Finland
ⁱ Present Address: Sodankyl Geophysical Observatory, University of Oulu, 90014 Oulu, Finland

of ^{245}Es, populated by the α decay of ^{249}Md. It should be noted that α-decay branching ratios and, to a lesser extent, half-lives are needed to deduce production cross sections. Finally, the measured production cross sections for ^{243}Es and ^{249}Md are discussed in the context of the $Z \simeq 100$ region and compared to the predictions of the KEWPIE2 statistical fusion-evaporation code [4].

II.   EXPERIMENTAL SETUP

The experiments were performed at the Accelerator Laboratory of the University of Jyväskylä (JYFL). The fusion-evaporation residues, including ^{243}Es and ^{249}Md, were separated from the fission fragments, the primary ^{48}Ca beam and the beam- and target-like reaction products using the Recoil Ion Transport Unit (RITU) gas-filled separator [5, 6], which was operated at a He pressure of 0.4 - 0.6 mbar. The RITU transmission is estimated to be approximately 30 % for the reactions considered here. The beam current was measured at regular intervals using a Faraday cup, and monitored using the detectors counting rate, thus allowing the beam dose to be deduced with an uncertainty of 20 %.

At the focal plane of RITU, the separated fusion-evaporation residues were first detected in a position-sensitive multi-wire proportional counter (MWPC) and then implanted in two adjacent double-sided silicon strip detectors (DSSDs), both detectors being part of the Gamma Recoil Electron Alpha-Tagging (GREAT) spectrometer [7]. The MWPC provided a time of flight (ToF) and energy loss (ΔE) measurement, allowing (i) selection of the fusion-evaporation residues using a ToF-ΔE identification matrix (ii) correlations with the DSSD, which enable the recoiling residues (coincidence) to be discriminated from the decay products (anti-coincidence). Each DSSD is 300 μm thick and consists of 60 × 40 strips with a 1 mm strip pitch. The Y side of the DSSD was calibrated using an external mixed ^{239}Pu, ^{241}Am, and ^{244}Cm α source. An energy offset is applied to account for the energy loss of the α particle in the detector entrance window (in case of external source), and for the daughter nucleus recoil (decay from the detector after implantation), so that the resulting energy corresponds to the literature value for the nuclei studied in the present work. The X side was amplified with a higher gain to measure low energy conversion electrons, and calibrated using an external ^{133}Ba source. Signals from all detectors were processed by a trigger-less acquisition system known as the Total Data Readout (TDR) [8]. The recoil decay correlation analysis was performed using the software package Grain [9]: after a first selection using the ToF-ΔE identification matrix, the fusion-evaporation residues (recoils) were identified using the energy of the α particles registered in the same pixel of the DSSD subsequent to the implantation of a recoil. The SAGE array [10] surrounded the target for the prompt gamma and conversion-electron detection, however data from this detector were not used in the present work.

III. ^{243}Es DECAY PROPERTIES AND PRODUCTION CROSS SECTION

A.   Decay and half-life measurement

The ^{243}Es isotope was discovered in the 1970s by Eskola $et\ al.$ using the ^{233}U(^{15}N,5n)^{243}Es reaction [11, 12], and latter revisited in the 1990s by Hatsukawa $et\ al.$, using the ^{233}U(^{14}N,4n)^{243}Es reaction [13]. A more recent study, performed with the SHIP separator at GSI by Antalic $et\ al.$ [14], has shown that ^{243}Es decays to its daughter via an α-particle with an energy of 7893 $\pm$ 10 keV, with a half-life of $T_{1/2} = 23 \pm 3$ s and a α-decay branching ratio of 61 $\pm$ 6 % . An α-particle fine structure was tentatively observed with peaks at 7745 $\pm$ 20 and 7850 $\pm$ 20 keV. In the work of Antalic $et\ al.$ ^{243}Es was populated in the decay of the mother nucleus ^{247}Md, while in the present study it was directly produced in the ^{197}Au(^{48}Ca,2n)^{243}Es reaction, with a 21 pnA ^{48}Ca beam at $\sim$ 210 MeV energy impinging on a ^{197}Au target. The ^{48}Ca + ^{197}Au reaction has already been studied in the 1990s by Gäggeler $et\ al.$ [15], however, few spectroscopic data were available at that time, preventing the discrimination of fusion-evaporation residues from 2n and 3n channels.

Fig. 1 presents the α-particle energy spectrum measured in the DSSD resulting from recoil-α correlations, with the decay of ^{243}Es clearly visible.
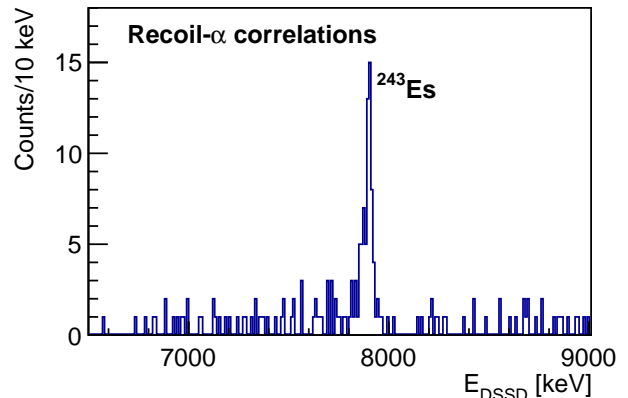

FIG. 1. Alpha-particle energy spectrum of ^{243}Es measured in the DSSD resulting from recoil-α correlations using a maximum search time of 268 s.

The time distribution (ΔT) of the α decay with respect to the implantation, selecting the ^{243}Es α-decay energy, is presented in Fig. 2. In the inset, the time distribution is drawn as a function of $ln(\Delta T)$ using a maximum search time of 10 h. The peak at $ln(\Delta T) = 10.5$ corresponds to the ^{243}Es decay, while that around $ln(\Delta T) = 16$ is related to random correlations occurring at an average

time interval of $\approx 5000\,\mathrm{s}$. The spectrum in the main panel can be fitted using the function [16]:

$$f(T) = Ae^{-(\lambda+r)\Delta T} + Be^{-r\Delta T}, \qquad (1)$$

where λ is the decay constant of the nucleus of interest and r is the random correlation rate. Similarly, the spectrum in the inset can be fitted following the method described in Ref. [17]. As expected, both procedures give the same result, yielding the half-life of $T_{1/2} = 24\pm3\,\mathrm{s}$, in agreement with the results of the experiment performed at SHIP [14].
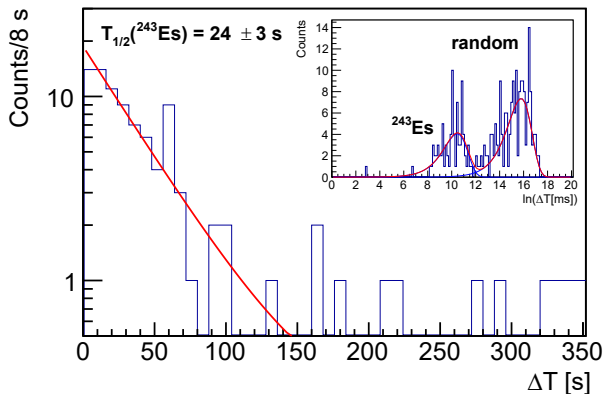

FIG. 2. Time distribution of α decays with respect to the ^{243}Es fusion-evaporation residue implantation. The inset shows the same data as a function of $ln(\Delta T)$, with ΔT expressed in ms. It should be noted that the scale is different for the two spectra: 350 s for the main panel, 135 h for the inset. The fit using a two-component decay curve (real and random) is shown is red.

The inset of Fig. 2 demonstrates that the ^{243}Es decay events can be well separated from the background in the defined range $ln(\Delta T) < 12.5$, which corresponds to a time window of 268 s after the recoil implantation. This search time is used in the next section in order to determine the number of events corresponding to the α decay of ^{243}Es.

The recoil-α-α correlations were used to search for the decay of ^{239}Bk following the ^{243}Es decay. The negative outcome of this search is again consistent with the results of the measurement at SHIP [14]. The decay properties of nuclei studied in the present work are summarized in Table I.

B. Production cross section

In order to study the production cross section for ^{243}Es using the fusion-evaporation reaction ^{197}Au(^{48}Ca,2n)^{243}Es, two different beam energies were used. The target used for this measurement was a $270 \pm 13\,\mu\mathrm{g\,cm^{-2}}$ thick ^{197}Au self-supporting foil. The cyclotron delivered a $213 \pm 1.0\,\mathrm{MeV}$ beam first passing

TABLE I. Summary of decay properties obtained in the present work compared to the literature values.

Nucleus	Half-life [s]	α-decay branching ratio [%]	Reference
^{243}Es	24 ± 3	^{239}Bk not observed	This work
	23 ± 3	61 ± 6	[14]
^{245}Es	65 ± 6	54 ± 7	This work
		40 ± 10	[18]
	80^{+96}_{-28}	80^{+20}_{-50}	[19]
	66 ± 6		[13]
	$55^{+12}_{-8.4}$		[20]
^{249}Md	26 ± 1	75 ± 5	This work
	25^{+14}_{-7}	> 60	[19]
	19^{+3}_{-2}		[21]
	$23.8^{+3.8}_{-2.9}$		[20]
	23 ± 3		[22]
		75	[23]

through the $100\,\mu\mathrm{g\,cm^{-2}}$ carbon window of the SAGE electron spectrometer. The first part of the study was performed with a beam energy in the Middle of the Target (MoT) estimated to be $210.0 \pm 1.0\,\mathrm{MeV}$. Then a carbon degrader foil of $100\,\mu\mathrm{g\,cm^{-2}}$ was placed upstream to reduce the incident energy (MoT) to $208.0 \pm 1.0\,\mathrm{MeV}$. The spectrum presented in Fig. 1 corresponds to the total statistics, namely with and without the degrader.

The number of counts attributed to the ^{243}Es α decay was obtained using a maximum search time of 268 s. The contribution from random correlations was estimated by integrating the random correlations component (second term in Eq. 1 in the case $\lambda \gg r$) using this time window. After subtracting this background, the number of α particles stemming from ^{243}Es was determined to be 50 ± 7 (32 ± 6) without (with) the carbon degrader foil. The uncertainties were evaluated following the method described in Ref. [24]. In the present work, the statistics is large enough to consider standard normal distributions, therefore symmetric uncertainties are adopted.

During the acquisition time without and with the degrader, the number of ^{48}Ca nuclei that impinged on the ^{197}Au target was equal to $(1.6 \pm 0.3) \times 10^{16}$ and $(1.2 \pm 0.2) \times 10^{16}$, respectively. Taking into account the ^{197}Au target thickness, the α-decay branching ratio of $61 \pm 6\,\%$ [14], the α-detection efficiency of 55%, and assuming a RITU transmission of 30%, a production cross section $\sigma(^{243}\mathrm{Es}) = 37 \pm 10\,\mathrm{nb}$ was deduced for a beam energy of $210.0 \pm 1.0\,\mathrm{MeV}$ (without degrader), and $\sigma(^{243}\mathrm{Es}) = 32\pm9\,\mathrm{nb}$ for a beam energy of $208.0\pm1.0\,\mathrm{MeV}$ (with degrader). Only statistical uncertainties corresponding to the beam dose, number of α-particles and α-decay branching ratio are given. The RITU transmission of 30% is actually a transmission $\times$ detection efficiency including the transmission through the separator, the time-of-flight and the DSSD detection efficiencies. The results are presented in Table II.

TABLE II. Production cross sections for ^{243}Es using the fusion-evaporation reaction ^{197}Au(^{48}Ca,2n)^{243}Es measured for two different ^{48}Ca beam energies (E$_{beam}$ corresponds to the middle of target). N$_\alpha$ is the number of observed α decays after background subtraction.

E$_{beam}$ [MeV]	^{48}Ca dose	N$_\alpha$	σ [nb]
210.0 ± 1.0	$(1.6 \pm 0.3) \times 10^{16}$	50 ± 7	37 ± 10
208.0 ± 1.0	$(1.2 \pm 0.2) \times 10^{16}$	32 ± 6	32 ± 9

IV. ^{249}Md DECAY PROPERTIES AND PRODUCTION CROSS-SECTION

The odd-Z nucleus ^{249}Md was populated using the fusion-evaporation reaction ^{203}Tl(^{48}Ca,2n)^{249}Md in three different irradiation campaigns. The first campaign was focused on cross-section measurements at two different bombarding energies of 214.3 ± 1.1 and 212.7 ± 1.1 MeV. The results are reported in section IV B. The two subsequent campaigns aimed principally at the in-beam and decay spectroscopy of ^{249}Md, results of which will be reported in a forthcoming publication. The data collected in the three campaigns were used to derive the ^{245}Es and ^{249}Md half-life and α-decay branching ratios, as presented in the following section.

A. ^{249}Md and ^{245}Es decay and half-life measurement

The α-particle energy spectra obtained using recoil-α and recoil-α-α correlations, with the statistics of the three campaigns summed together, are presented in Fig. 3. A maximum search time of 10 min after the identification of an implanted recoiling nucleus was used. ^{249}Md features an electron capture (EC)/β^+ decay branch feeding ^{249}Fm. The α decay of the latter is observed using recoil-α correlations since the detection system is insensitive to the β^+ particle (see the upper panel of Fig. 3). The ^{245}Es α decay observed using recoil-α correlations corresponds to the events when the α particle emitted from ^{249}Md escapes from the DSSD without being detected. The α decay of ^{249}Fm is more clearly visible in Fig. 4, which represents the α-decay time in a logarithmic scale as a function of the α-particle energy. Using recoil-α-α correlations allows the mother, ^{249}Md and daughter, ^{245}Es α decays to be isolated as shown in middle and bottom panels of Fig. 3. From the literature, the α-particle energies are: E$_\alpha$(^{249}Md)= 8026 ± 10 keV [22], and E$_\alpha$(^{245}Es)= 7730 ± 1 keV [13]. The satellite peaks in the α decay of ^{249}Md at 7956 and 8087 keV, suggested in [22], are also tentatively observed in the present work.

Figure 5 shows the time distribution of the ^{249}Md α decay with respect to the implantation time. The distribution plotted as a function of $ln(\Delta T)$ for a maximum search time of 24 h is shown in the inset. As shown in
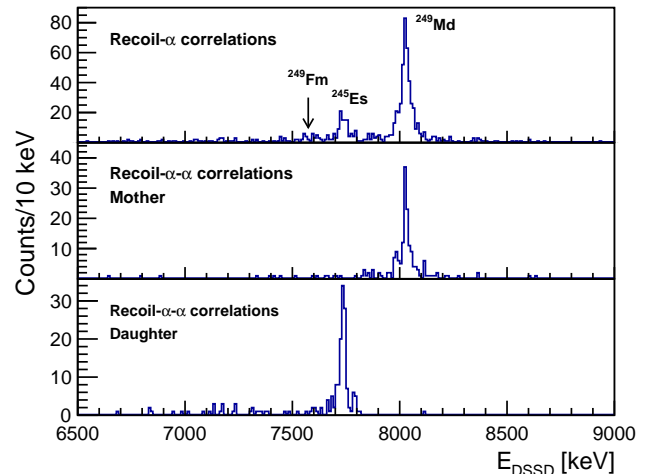

FIG. 3. Alpha-particle energy spectra of ^{249}Md, ^{249}Fm and ^{245}Es resulting from recoil-α and recoil-α-α correlations using a maximum search time of 10 min.
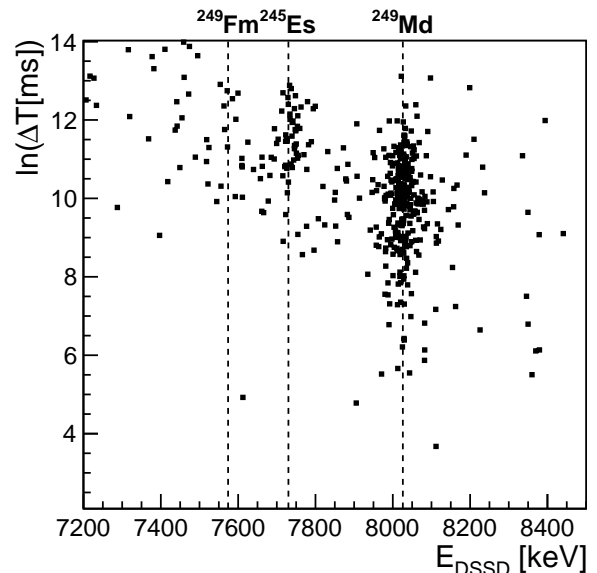

FIG. 4. Alpha-decay time distribution in a logarithmic scale (from ~ 7 ms to ~ 20 min) as a function of the decay energy.

this plot, the random correlations are negligible, therefore the time distribution displayed in the main panel can be fitted with a single exponential function. A half-life $T_{1/2} = 26 \pm 1$ s is obtained using a maximum search time of 300 s. This value can be compared with previously measured half-lives. The ^{249}Md decay has been studied at SHIP by Hessberger et al. following the α decay of ^{257}Db ($\rightarrow ^{253}$Lr $\rightarrow ^{249}$Md) [19, 21] and the α decay of ^{253}Lr [22], and by Gates et al. using the Berkeley Gas-Filled Separator following the α decay of ^{257}Db [20]. Our revised half-life of ^{249}Md obtained via direct production and with higher statistics is compatible with the values obtained in these works: 25^{+14}_{-7} s [19], 19^{+3}_{-2} s [21],

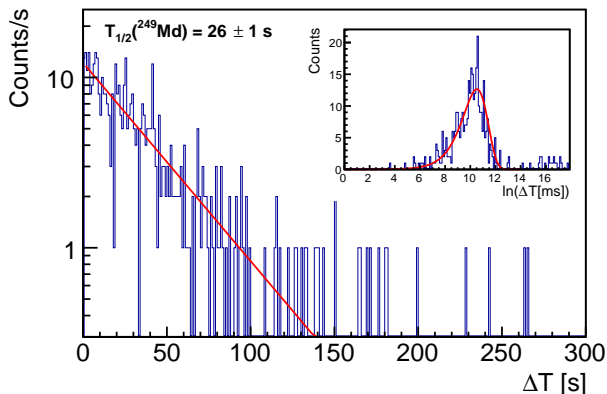23 ± 3 s [22], $23.8^{+3.8}_{-2.9}$ s [20]; see also Table I.

FIG. 5. Time distribution of α decays with respect to the ^{249}Md fusion-evaporation residue implantation. The inset shows the same data as a function of $ln(\Delta T)$, with ΔT expressed in ms. It should be noted that the scale is different for the two spectra: 300 s for the main panel, 18.2 h for the inset. The fit using a one-component decay curve is shown in red.

Similarly, Fig. 6 presents the time distribution of the ^{245}Es α decay with respect to that of ^{249}Md, the time represented in both linear and as a function of $ln(\Delta T)$ scales. Again, the background is found to be negligible. The distribution was then fitted with a single component. The half-life $T_{1/2}(^{245}\text{Es}) = 65 \pm 6$ s was extracted, a value compatible with those obtained by Hessberger et al. following α decay of ^{257}Db ($\rightarrow\, ^{253}$Lr $\rightarrow\, ^{249}$Md $\rightarrow\, ^{245}$Es): 80^{+96}_{-28} s [19], by Hatsukawa et al. after direct synthesis using the fusion-evaporation reactions ^{238}U$(^{14}$N,$7n)^{245}$Es and ^{237}Np$(^{12}$C,4n$)^{245}$Es: 66 ± 6 s [13], and by Gates et al. following α decay of ^{257}Db: $55^{+12}_{-8.4}$ s [20]; see also Table I.

The α-decay branching ratio of ^{249}Md is defined as the ratio of the α-decay branch to ^{245}Es to the total decay strength, including the EC/β^+ branch to ^{249}Fm. The latter is evaluated using the number of events attributed to the ^{249}Fm α decay from Figs. 3 and 4, corrected for the ^{249}Fm α-decay branching ratio. A correction is also applied to take into account the fraction of ^{249}Fm nuclei that decay during the search time of 600 s. The ^{249}Fm half-life of 2.6 ± 0.7 min is taken from the evaluated data [25]. The ^{249}Fm α-decay branching ratio of 15.6 ± 1.0 % is taken from Hessberger et al. [26], which is more recent that the evaluation of Ref. [25][1]. The resulting α-decay branching ratio deduced in the present
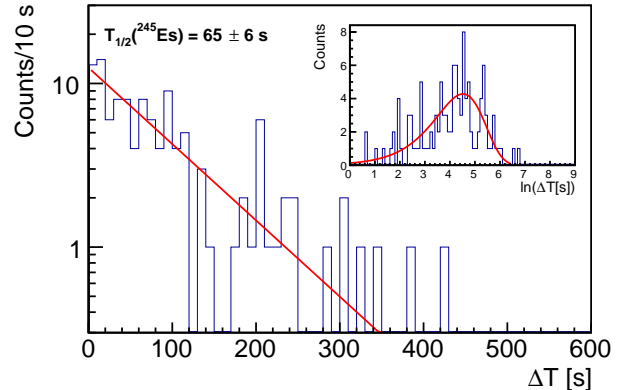
work is $b_\alpha(^{249}\text{Md}) = 75 \pm 5$ %. The evaluated value of $b_\alpha(^{249}\text{Md}) > 60$ % [25] corresponds to the measurement of Hessberger et al., which has been obtained in the study of the ^{257}Db decay chain [19]. A more recent value of $b_\alpha(^{249}\text{Md}) = 75$ %, quoted without uncertainty in the PhD thesis of B. Streicher [23], is in perfect agreement with our measurement; see also Table I.

The α-decay branching ratio of ^{245}Es can be extracted in two distinct ways. The first possibility is to derive it as the ratio of the number of events corresponding to ^{249}Md obtained using recoil-α-α and recoil-α correlations, corrected for the DSSD efficiency for a full-energy measurement $\epsilon_\alpha = 55$ %, under the condition that the recoil-α-α correlations are obtained by gating on the full-energy peaks only:

$$b_\alpha(^{245}\text{Es}) = \frac{N_{\text{recoil}-\alpha-\alpha}(^{249}\text{Md})}{N_{\text{recoil}-\alpha}(^{249}\text{Md})} \frac{1}{\epsilon_\alpha}. \qquad (2)$$

The second option is to obtain it as the ratio of counts corresponding to ^{245}Es and ^{249}Md in the total α-particle spectrum. Both methods lead to the same value of $b_\alpha(^{245}\text{Es}) = 54 \pm 7$ %. For comparison, the previously reported values were $b_\alpha(^{245}\text{Es}) = 40 \pm 10$ % (Eskola et al. [18]), $b_\alpha(^{245}\text{Es}) = 80^{+20}_{-50}$ % (Hessberger et al. [19]). The decay properties of ^{249}Md and ^{245}Es are summarized in Table I.

B. Production cross section

The fusion-evaporation reaction ^{203}Tl$(^{48}$Ca,$2n)^{249}$Md was studied at two different bombarding energies. The cyclotron delivered a 218 MeV beam first passing through the 100 μg cm^{-2} carbon window of the SAGE electron spectrometer. The ^{203}Tl target having a thickness of

---

[1] It should be noted that in Ref. [26], the half-life of ^{249}Fm has not been re-measured. The value adopted in this reference is actually that of the evaluation Ref. [25], i.e. 2.6 ± 0.7 min. In the most recent Nubase2016 evaluation [27], the α-decay branching ratio of ^{249}Fm is taken from Ref. [25] (33 ± 9 %) while for the half-life only the value from [28] (96 ± 6 s) is selected.

FIG. 6. Time distribution of α decay of ^{245}Es with respect to the ^{249}Md α decay. The inset shows the same data as a function of $ln(\Delta T)$, with ΔT expressed in s. It should be noted that the scale is different for the two spectra: 600 s for the main panel, 2.25 h for the inset. The fit using a one-component decay curve is shown is red.

$318 \pm 16 \, \mu\mathrm{g}\,\mathrm{cm}^{-2}$ was evaporated on a carbon foil of $20 \, \mu\mathrm{g}\,\mathrm{cm}^{-2}$, and covered by a $10 \, \mu\mathrm{g}\,\mathrm{cm}^{-2}$ carbon protection layer. The resulting energy in the middle of the ^{203}Tl target was estimated to be 214.3 ± 1.1 MeV. Using in addition a $80 \, \mu\mathrm{g}\,\mathrm{cm}^{-2}$ carbon degrader foil resulted in an energy of 212.7 ± 1.1 MeV MoT.

The spectra were obtained using a search time of 207 s i.e. eight ^{249}Md half-lives. Contrary to the ^{243}Es case, the background was found to be negligible.

The total number of ^{48}Ca particles that impinged on the target was $(1.8 \pm 0.4) \times 10^{15}$ $((1.5 \pm 0.3) \times 10^{15})$ for the measurement without (with) carbon degrader foil. Using a ^{203}Tl target thickness of $318 \pm 16 \, \mu\mathrm{g}\,\mathrm{cm}^{-2}$, an α branching ratio of $75 \pm 5\,\%$, a RITU transmission $\times$ detection efficiency of $30\,\%$ and a full-energy α-detection efficiency of $55\,\%$, cross sections $\sigma(^{249}\mathrm{Md})$ of 300 ± 80 nb and 70 ± 40 nb are deduced for the incident energies of 214.3 and 212.7 MeV, respectively. Again, only statistical uncertainties are given. The results are summarized in Table III.

TABLE III. Production cross sections for ^{249}Md using the fusion-evaporation reaction ^{203}Tl(^{48}Ca,2n)^{249}Md measured for two different ^{48}Ca beam energies (E_{beam} corresponds to the middle of the target).

E_{beam} [MeV]	^{48}Ca dose	N_α	σ [nb]
214.3 ± 1.1	$(1.8 \pm 0.4) \times 10^{15}$	63 ± 8	300 ± 80
212.7 ± 1.1	$(1.5 \pm 0.3) \times 10^{15}$	12 ± 4	70 ± 40

V. DISCUSSION

In this section we discuss the new cross-section measurements for ^{243}Es and ^{249}Md. These results are placed in the context of experimental cross sections for cold fusion-evaporation reactions, 2n channel, for $Z \approx 100$, presented in Fig. 7, and compared to new reactions dynamics calculations using the statistical fusion-evaporation code KEWPIE2 [4].

A. 2n channel fusion-evaporation systematics

It is generally acknowledged that the fusion-evaporation reactions can be described as three subsequent independent processes: capture, compound-nucleus formation, and survival of the residual nucleus. The description of the capture step is rather well controlled in terms of barrier penetration, with no rapid evolution as a function of mass and charge when using similar projectiles and targets. The formation step results in a sharp decrease of the cross section for projectile-target combinations with $Z_p Z_t \gtrsim 1600 - 1800$, known as the fusion hindrance, which prevents the formation of a compound nucleus by leading the di-nuclear composite

towards quasi-fission route. This effect starts to act in the region considered here, and it can account for the exponential decrease of the cross sections observed for larger Z values in Fig. 7. Consequently, only the survival step can account for the decrease of cross sections below $Z \approx 102$. The global trend displayed by the cross sections presented in Fig. 7 may be explained by a combination of two effects. First, the four-fold magic character of the ^{48}Ca $+$ ^{208}Pb $\rightarrow$ ^{256}No* reaction leads to a low Q value and therefore a higher survival probability in the evaporation and de-excitation processes. This enhancement is observed for ^{254}No and neighbouring residual nuclei. Second, the semi-magicity at $Z = 100$, $N = 152$ leads to higher shell corrections (higher fission barrier) and therefore higher survival probability around ^{252}Fm. Note that if the cross sections are plotted as a function of the mass or neutron number, they also display a bell-shaped behaviour.

B. Cross-section calculations

In the following, the fusion-evaporation cross sections illustrated with the new experimental results for ^{243}Es and ^{249}Md are discussed in terms of survival from the compound to the residual nucleus, with an emphasis on the effect of the fission barrier. The present measurements are performed in a mass region where the fusion hindrance is not yet significant. Consequently, the fusion process is modelled in the KEWPIE2 code by considering only the capture phase, which is computed using a proximity potential and the Wentzel-Kramers-Brillouin (WKB) approximation, see Ref. [4] for details.

The KEWPIE2 code [4] treats the competition between light-particle evaporation and fission, which occurs within an excited compound nucleus, using the statistical formalisms of Weisskopf [41] and Bohr-Wheeler [42], respectively. The entire set of default parameters used in the KEWPIE2 code is presented in Ref. [4]. In the following we will only focus on a few parameters, which are not well-defined either theoretically or experimentally in this mass region [43]. These parameters are the reduced friction parameter β, the shell-damping energy E_d and the shell corrections ΔE_{sh}. These parameters are related, respectively, to the viscosity of nuclear matter, the stability of shell corrections with temperature and the fission-barrier height, following Eq. 3 for the latter:

$$B_f = B_{LDM} - \Delta E_{sh}, \tag{3}$$

where B_f is the fission-barrier height and B_{LDM} the liquid-drop fission barrier. The default values used in the KEWPIE2 code are $\beta = 2 \times 10^{21}$ s^{-1}, $\mathrm{E}_d = 19$ MeV, while the finite-range droplet model (FRDM) ΔE_{sh} shell corrections are taken from Ref. [44]. It should be stressed that those parameters mainly affect the fission process that is known to be dominant for heavy and super-heavy nuclei. Indeed, a small variation of the fission parameters, such as the strength of the dissipation or the fission-
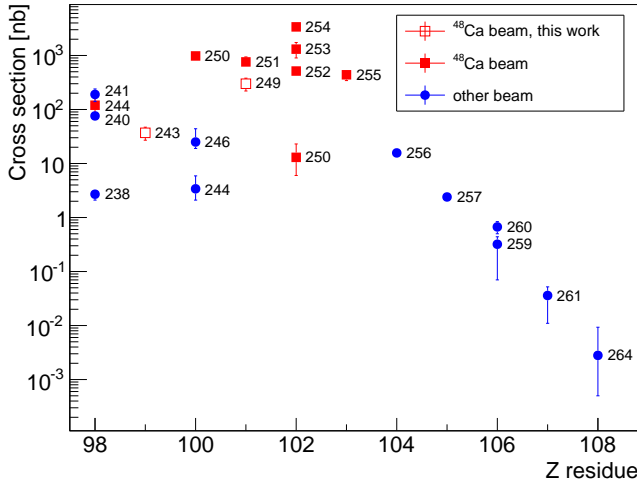
FIG. 7. Systematics of fusion-evaporation cross sections in the $2n$ channel as a function of Z of the residual nucleus. The red squares correspond to reactions induced by a ^{48}Ca beam, while blue circles to those using other beams. The new ^{243}Es and ^{249}Md measurements are denoted by empty square symbols. The mass number A of the residual nucleus is given to the right of each symbol. Data are taken from Refs. [29] (^{238,240,241}Cf), [30] (^{244}Cf), this work (^{243}Es, ^{249}Md), [31] (^{244,246}Fm), [32] (^{250}Fm), [33] (^{251}Md), [34] (^{250}No) [35] (^{252,253}No) [36] (^{254}No, ^{255}Lr), [37] (^{256}Rf), [21] (^{257}Db), [38] (^{259}Sg), [22] (^{260}Sg), [39] (^{261}Bh), [40] (^{264}Hs).

FIG. 8. Top: Comparison between the experimental production cross sections for ^{243}Es obtained in the present paper, and the calculations of the $1n$, $2n$ and $3n$ cross sections performed with the KEWPIE2 code using the default parameters (macroscopic part described by the Thomas-Fermi parametrization as proposed by Myers-Swiatecki [45], and the microscopic part based on the FRDM shell corrections [44]). Bottom: same for ^{249}Md.

barrier heights, leads to a significant modification of the survival probability and, consequently, the related observables, in particular the production cross sections.

Figure 8 presents the experimental results for the production cross sections for ^{243}Es and ^{249}Md (Tables II and III) compared to the calculations performed with the KEWPIE2 code using the default parameters. For ^{249}Md, the calculation reproduces the measured production cross sections well, while it underestimates them by a factor of 5 for the ^{243}Es case. The discrepancy for this latter case cannot be explained by a failure of the fusion model. Indeed, for a beam energy corresponding to the present measurement ($E_{cm} \approx 169\,\mathrm{MeV}$), the fusion model provides a fusion cross section $\sigma_{fus} = 55\,\mathrm{mb}$ in good agreement with the measurement $\sigma_{fus} = 42\,\mathrm{mb}$ of Ref. [46]. Moreover, a discussion of the fusion cross-section for the ^{48}Ca+^{208}Pb reaction, for which the WKB approximation provides a good description without fusion hindrance considerations, can be found in Ref. [4]. In Fig. 9, the fission-barrier heights or the reduced friction parameters have been increased in order to reproduce the measurements for the $2n$ evaporation channel. Concerning the fission-barrier heights, it is necessary to add 500 keV to the absolute value of the shell corrections (with the liquid-drop fission barrier kept unchanged, see Eq. 3), to obtain a good agreement between the calculations and the data. Furthermore, the reduced friction parameter has to be increased by a factor of three, i.e.
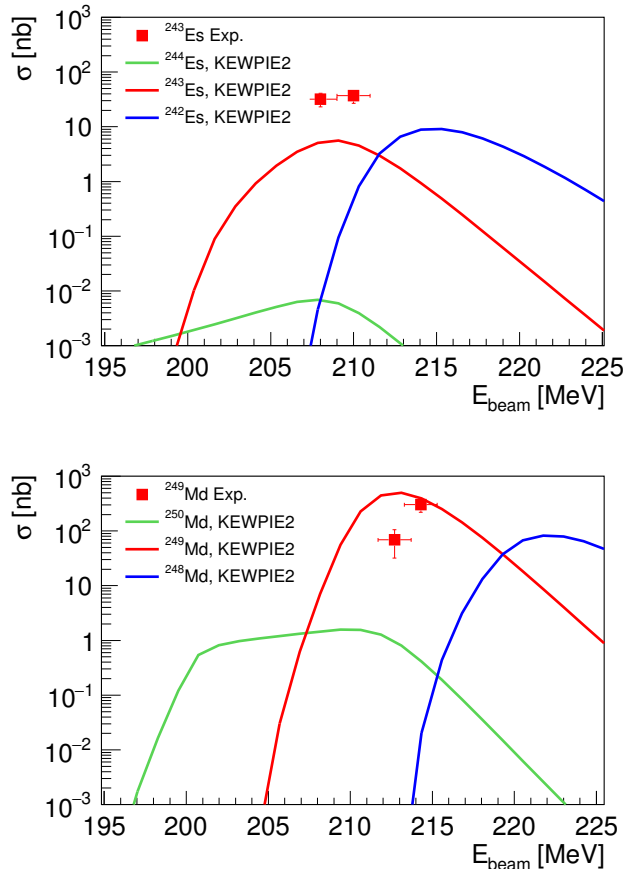
to $\beta = 6 \times 10^{21}\,\mathrm{s}^{-1}$, in order to obtain the same agreement. It should be stressed that these adjustments remain within the uncertainty intervals for these parameters, as discussed in Refs. [4, 43]. Moreover, no theoretical model can presently predict the fission-barrier heights with an accuracy better than $0.5 - 1\,\mathrm{MeV}$ [47–49]. In the super-heavy nuclei region, differences between the models can be as large as $4\,\mathrm{MeV}$ [50]. Consequently, we cannot attribute the discrepancy observed for ^{243}Es (Fig. 8) to any specific parameters used in the KEWPIE2 code, neither to any inputs from other nuclear models, in particular those related to the fission process. Hence, the measured production cross sections for the ^{243}Es and ^{249}Md isotopes can be fully explained within the uncertainties in nuclear models and phenomenological parametrizations implemented in the KEWPIE2 code.

Figure 9 also shows the influence of the modification of the shell corrections, or the reduced friction param-
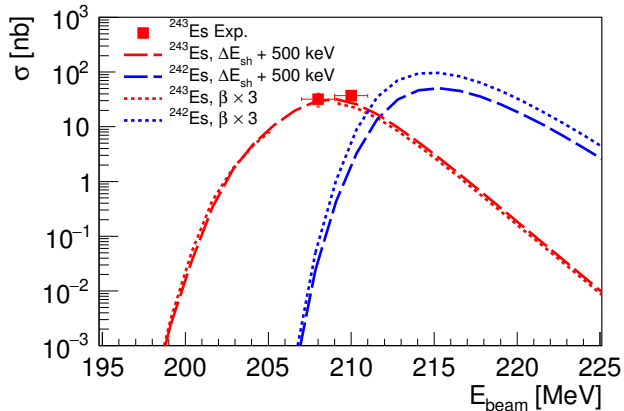
FIG. 9. Comparison between the experimental production cross sections for ^{243}Es extracted in the present paper, and the calculations performed with the KEWPIE2 code considering either an adjustment of +500 keV of the barrier heights, or an adjustment of the reduced friction parameter to $\beta = 6 \times 10^{21}\,\mathrm{s}^{-1}$.

eter, on the $3n$ evaporation channel, which corresponds to the production of the ^{242}Es isotope. A discrepancy of a factor of two between the two calculations is observed. Moreover, a modification of the reduced friction parameter has a stronger effect on the $3n$ channel than a modification of the shell corrections. Since the latter are temperature-dependent via Ignatyuk's prescription [51], their influence on the survival probability decreases with increasing temperature. In contrast, the reduced friction parameter affects the fission width $\Gamma_f^{(A)}$ of all (A, Z) isotopes equally, via the Kramers factor K [52]:

$$\Gamma_f^{(A)} \propto (K \times \Gamma_f^{BW}(T))^{(A)}, \tag{4}$$

with

$$K = \sqrt{1 + \left(\frac{\beta}{2\omega_{\mathrm{SD}}}\right)^2} - \frac{\beta}{2\omega_{\mathrm{SD}}}, \tag{5}$$

where Γ_f^{BW} is the Bohr-Wheeler fission width [42], β is the reduced friction parameter and ω_{SD} is the potential curvature at the saddle point. Since fission is the dominant process in the heavy and super-heavy mass region, the survival probability of a specific xn evaporation channel can be expressed according to a power law of the Kramers factor:

$$P_{xn} \approx \left(\frac{1}{K}\right)^x \prod_{i=0}^x \frac{\Gamma_n^{(A-i)}}{(\Gamma_f^{BW})^{(A-i)}}. \tag{6}$$

The discrepancy already observed in Fig. 9 for the predictions for the $3n$ evaporation channel will increase further with the number of evaporated neutrons, due to the power law of the Kramers factor. Consequently, it should

be stressed that, in order to provide meaningful constraints on the code parameters, accurate cross-section measurements are needed for various evaporation channels, as well as for many different incident energies.

It should be mentioned that a systematic comparison of the predictions of the KEWPIE2 code with existing experimental data for actinides and transactinides has been attempted in Ref. [4], considering $1n$ to $6n$ evaporation channels for which a good agreement has always been found with standard parameters. So far, no constraint on the reduced friction parameter, neither on the fission-barrier height could be deduced from this systematic study due to the lack of precise measurements. On the other hand, an uncertainty of 1 MeV in the fission-barrier height translates into an uncertainty of about one order of magnitude in the survival probability for the heavy and super-heavy mass regions. In order to solve this issue and eventually provide a deeper understanding of reaction mechanisms involved in the synthesis of heavy and super-heavy nuclei, the fission barriers should be precisely measured, which will help to reduce the sensitivity of statistical codes like KEWPIE2 to the fission parameter uncertainties.

In practice, fission barriers can be determined by measuring the fission probability as a function of the excitation energy using neutron-induced or surrogate reactions. However, these techniques are limited to $Z \leq 100$ by the availability of required targets [47]. Recently, the fission barrier has been measured in a heavier nucleus, ^{254}No, for the first time by Henning et al. [53]. This was possible thanks to a different approach, namely measuring the γ-ray decay probability P_γ as a function of the excitation energy after a fusion-evaporation reaction. P_γ was measured using the Gammasphere germanium array at the Argonne National Laboratory in the calorimetric mode. The relation:

$$P_{fission} = 1 - P_\gamma \tag{7}$$

after the last neutron evaporation yields the fission probability $P_{fission}$ as a function of the excitation energy. A fission barrier $B_f = 6.6$ MeV in ^{254}No has been deduced from this experiment, associated with a 0.9 MeV uncertainty, which remains too large to provide an additional constraint on the fission barrier height parameter in the KEWPIE2 code. It should be noted that the reaction ^{208}Pb$(^{48}$Ca$,2n)^{254}$No is one of the reaction that has been used to benchmark the KEWPIE2 code [4]. Using the FRDM shell corrections of Ref. [44] (corresponding to a fission barrier height of 5.05 MeV), the excitation function is well reproduced by slightly changing the default parameters, namely either decreasing the friction parameter β by about 80 %, or decreasing the shell-damping energy E_d by about 30 %, which is well within the uncertainties of the model. The precision on the fission barrier height achieved with the method of Ref. [53] is mainly related to the statistics. In the future, better accuracy could be achieved with a large coverage gamma tracking array coupled to a high acceptance recoil separator.

In addition, the technique of entry distribution measurement provides not only the fission barrier at zero angular momentum, but its evolution as a function of the spin.

As stated above, in the KEWPIE2 code the fission barrier is approximated by the sum of the liquid-drop component and of the ground-state shell correction (Eq. 3). The macroscopic part is described by the Thomas-Fermi parametrization as proposed by Myers-Swiatecki [45], and the microscopic part is based on the FRDM shell corrections [44]. The calculated fission barriers for all isotopes leading to the production of ^{243}Es and ^{249}Md, including their macroscopic and microscopic parts, are listed in Table IV. The agreement between the calculations and the present measurements (Fig. 8) confirms that the FRDM shell corrections combined with the Myers-Swiatecki liquid-drop parametrization provide a good estimate of the fission barriers. The same statement was made in Ref. [48] for actinides, and it is also consistent with the systematics presented in Ref. [4] for benchmarking the KEWPIE2 code for actinides and transactinides up to nobelium isotopes. Nevertheless, the fission barriers for ^{243}Es (3.5 MeV) and ^{249}Md (4.2 MeV) used in the calculations are at least 2 MeV lower than those resulting from recent calculations based on macroscopic-microscopic approaches, i.e. by Möller et al. [54, 56] and Jachimowicz et al. [55], see Table IV.

The production cross section for ^{243}Es, calculated assuming the fission barrier from Ref. [54], is presented in Fig. 10. Since Ref. [54] provides only the total fission barrier, we assumed that the liquid-drop component is still described by the Myers-Swiatecki liquid drop parametrization, the difference being the microscopic part according to Eq. 3. As shown in Fig. 10, the calculation overestimates the data by two orders of magnitude, and no adjustment of the KEWPIE2 parameters can significantly improve the agreement. This shows that the recent calculations of fission barriers based on macroscopic-microscopic approaches [54, 55] are difficult to reconcile with the well-established statistical formalisms of Weisskopf and Bohr-Wheeler to assess the survival probability. The present work therefore points out the urgent need for more fission barrier measurements and modelling in the heavy and super-heavy mass region.

A way to provide constraints on the parameters used in the KEWPIE2 code would be to perform more precise measurements in the very-heavy and super-heavy nuclei mass region for a whole set of different evaporation channels, including a large scan in excitation energy for each of them. Indeed, using relevant data can help to fix and/or eliminate the impact of a specific parameter.

Firstly, fission-barrier heights can be constrained using a statistical analysis of excitation functions based on the Bayesian inference, as shown in [4, 57]. This is possible since the fission barrier is the parameter which has the strongest impact on the fusion-evaporation cross section. Secondly, using the excitation function allows the fission-barrier height and reduced friction parameter to be fixed for a specific isotope. Such a procedure may allow the
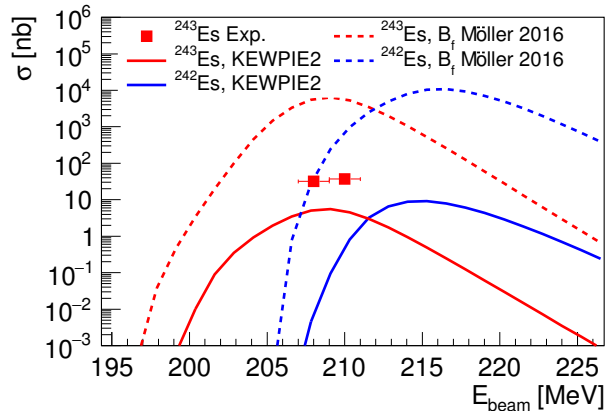

FIG. 10. Comparison between experimental production cross sections for ^{243}Es obtained in the present paper, and calculations done with the KEWPIE2 code considering either the 2016 fission barrier from Möller et al. [56] (dotted lines), or the standard KEWPIE2 parameters (solid lines).

energy dependence of Ignatyuk's prescription that controls the shape of the excitation function to be checked and improved upon. Thirdly, comparing two evaporation channels in the same reaction would enable a constraint to the reduced friction parameter, as explained above and shown in Fig. 9. Only by combining these different methods, one may expect to reduce the uncertainties on the modelling of fusion-evaporation reactions and providing robust constraints on the key parameters.

VI. CONCLUSION

The odd-Z ^{243}Es and ^{249}Md were produced in the ^{197}Au(^{48}Ca,$2n$)^{243}Es and ^{203}Tl(^{48}Ca,$2n$)^{249}Md fusion-evaporation reactions, respectively. The half-life of ^{243}Es, ^{249}Md and its daughter ^{245}Es were measured and the results were found compatible with those obtained in previous measurements following α-decay of heavier nuclei. The precision of the half-lives of ^{249}Md and ^{245}Es was increased, as well as those of the α-decay branching ratios for those nuclei.

Production cross-sections of ^{243}Es and ^{249}Md have been measured for the first time using ^{48}Ca-induced reactions, and compared to the calculations performed with the KEWPIE2 code [4]. A good agreement was found within the existing uncertainties in the key parameters related to the fission path, namely the reduced friction parameter, the shell-damping energy and the fission-barrier height. In particular, the sensitivity of the production cross-section to the fission-barrier height has been emphasized, pointing out the need of fission-barrier experimental data with higher precision in order to further constrain the KEWPIE2 code and, more generally, fission dynamics calculations.

TABLE IV. Fission barriers B_f, liquid-drop barriers B_{LDM} and shell corrections ΔE_{sh} for the isotopes of interest, calculated using the KEWPIE2 code and macroscopic-microscopic approaches [54, 55].

Isotope	B_f (MeV) KEWPIE2 (Eq. 3)	B_{LDM} (MeV) [45]	ΔE_{sh} (MeV) [44]	B_f (MeV) [54]	B_f (MeV) [55]
^{245}Es	4.21	0.95	-3.26	6.53	7.25
^{244}Es	4.14	0.92	-3.22	6.28	7.72
^{243}Es	3.53	0.90	-2.64	5.98	6.72
^{242}Es	3.44	0.87	-2.58	5.70	7.01
^{251}Md	4.78	0.55	-4.23	6.98	7.09
^{250}Md	4.63	0.53	-4.10	6.70	7.45
^{249}Md	4.19	0.51	-3.68	6.24	6.72
^{248}Md	4.08	0.49	-3.59	6.03	6.94

[1] D. Ackermann and C. Theisen, Physica Scripta 92, 083002 (2017).

[2] M. Asai, F. Heßberger, and A. Lopez-Martens, Nucl. Phys. A 944, 308 (2015).

[3] C. Theisen, P. T. Greenlees, T.-L. Khoo, P. Chowdhury, and T. Ishii, Nucl. Phys. A 944, 333 (2015).

[4] H. Lü, A. Marchix, Y. Abe, and D. Boilley, Comput. Phys. Commun. 200, 381 (2016).

[5] M. Leino, J. Äystö, T. Enqvist, P. Heikkinen, A. Jokinen, M. Nurmia, A. Ostrowski, W. Trzaska, J. Uusitalo, K. Eskola, P. Armbruster, and V. Ninov, Nucl. Instrum. Methods Phys. Res. B 99, 653 (1995).

[6] J. Sarén, J. Uusitalo, M. Leino, and J. Sorri, Nucl. Instrum. Methods Phys. Res. A 654, 508 (2011).

[7] R. D. Page, A. N. Andreyev, D. E. Appelbe, P. A. Butler, S. J. Freeman, P. T. Greenlees, R.-D. Herzberg, D. G. Jenkins, G. D. Jones, P. Jones, et al., Nucl. Instrum. Methods Phys. Res. B 204, 634 (2003).

[8] I. H. Lazarus, D. E. Appelbe, P. A. Butler, P. J. Coleman-Smith, J. R. Cresswell, S. J. Freeman, R. D. Herzberg, I. Hibbert, D. T. Joss, S. C. Letts, et al., IEEE Trans. Nucl. Sci. 48, 567 (2001).

[9] P. Rahkila, Nucl. Instrum. Methods Phys. Res. A 595, 637 (2008).

[10] J. Pakarinen, P. Papadakis, J. Sorri, R. D. Herzberg, P. T. Greenlees, P. A. Butler, P. J. Coleman-Smith, D. M. Cox, J. R. Cresswell, P. Jones, et al., Eur. Phys. J. A 50, 53 (2014).

[11] P. Eskola, K. Eskola, M. Nurmia, and A. Ghiorso, "Two new isotopes of einsteinium, ^{243}Es and ^{244}Es," LBL-2315 Preprint (1972).

[12] P. Eskola, K. Eskola, M. Nurmia, and A. Ghiorso, Physica Fennica 8, 357 (1973).

[13] Y. Hatsukawa, T. Ohtsuki, K. Sueki, H. Nakahara, I. Kohno, M. Magara, N. Shinohara, H. L. Hall, R. A. Henderson, C. M. Gannet, et al., Nucl. Phys. A 500, 90 (1989).

[14] S. Antalic, F. P. Heßberger, S. Hofmann, D. Ackermann, S. Heinz, B. Kindler, I. Kojouharov, P. Kuusiniemi, M. Leino, B. Lommel, R. Mann, and Š. Šáro, Eur. Phys. J. A 43, 35 (2010).

[15] H. W. Gäggeler, D. T. Jost, A. Türler, P. Armbruster, W. Brüchle, H. Folger, F. P. Heßberger, S. Hofmann, G. Münzenberg, V. Ninov, et al., Nucl. Phys. A 502, 561 (1989).

[16] M. E. Leino, S. Yashita, and A. Ghiorso, Phys. Rev. C 24, 2370 (1981).

[17] K. H. Schmidt, Eur. Phys. J. A 8, 141 (2000).

[18] P. Eskola, Phys. Rev. C 7, 280 (1973).

[19] F. P. Heßberger, G. Münzenberg, S. Hofmann, Y. K. Agarwal, K. Poppensieker, W. Reisdorf, K. H. Schmidt, J. R. H. Schneider, W. F. W. Schneider, H. J. Schött, et al., Z. Phys. A 322, 557 (1985).

[20] J. M. Gates, S. L. Nelson, K. E. Gregorich, I. Dragojević, C. E. Düllmann, P. A. Ellison, C. M. Folden III, M. A. Garcia, L. Stavsetra, R. Sudowe, D. C. Hoffman, and H. Nitsche, Phys. Rev. C 78, 034604 (2008).

[21] F. P. Heßberger, S. Hofmann, D. Ackermann, V. Ninov, M. Leino, G. Münzenberg, S. Saro, A. Lavrentev, A. G. Popeko, A. V. Yeremin, et al., Eur. Phys. J. A 12, 57 (2001).

[22] F. Heßberger, S. Hofmann, B. Streicher, B. Sulignano, S. Antalic, D. Ackermann, S. Heinz, B. Kindler, I. Kojouharov, P. Kuusiniemi, et al., Eur. Phys. J. A 41, 145 (2009).

[23] B. Streicher, Synthesis and spectroscopic properties of Synthesis and spectroscopic properties of transfermium isotopes with Z = 105, 106 and 107, Ph.D. thesis, Faculty of mathematics, physics and informatics. Cornelius University. Bratislava (2006).

[24] W. Brüchle, Radiochim. Acta 91, 71 (2003).

[25] K. Abusaleem, Nucl. Data Sheets 112, 2129 (2011).

[26] F. P. Heßberger, S. Antalic, D. Ackermann, Z. Kalaninová, S. Heinz, S. Hofmann, B. Streicher, B. Kindler, I. Kojouharov, P. Kuusiniemi, *et al.*, Eur. Phys. J. A **48**, 75 (2012).

[27] G. Audi, F. G. Kondev, M. Wang, W. Huang, and S. Naimi, Chinese Physics C **41**, 030001 (2017).

[28] Heßberger, F. P., Hofmann, S., Ackermann, D., Cagarda, P., Herzberg, R. -D., Kojouharov, I., Kuusiniemi, P., Leino, M., and Mann, R., Eur. Phys. J. A **22**, 417 (2004).

[29] J. Khuyagbaatar, F. P. Heßberger, S. Hofmann, D. Ackermann, V. S. Comas, S. Heinz, J. A. Heredia, B. Kindler, I. Kojouharov, B. Lommel, *et al.*, Eur. Phys. J. A **46**, 59 (2010).

[30] J. Konki, B. Sulignano, P. T. Greenlees, C. Theisen, K. Auranen, H. Badran, R. Briselet, D. M. Cox, F. Defranchi Bisso, J. Dobaczewski, *et al.*, Phys. Rev. C **97**, 024306 (2018).

[31] H. Gäggeler, T. Sikkeland, G. Wirth, W. Brüchle, W. Bögl, G. Franz, G. Herrmann, J. V. Kratz, M. Schädel, K. Sümmerer, and W. Weber, Z. Phys. A **316**, 291 (1984).

[32] J. E. Bastin, R.-D. Herzberg, P. A. Butler, G. D. Jones, R. D. Page, D. G. Jenkins, N. Amzal, P. M. T. Brew, N. J. Hammond, R. D. Humphreys, *et al.*, Phys. Rev. C **73**, 024308 (2006).

[33] A. Chatillon, C. Theisen, E. Bouchez, P. A. Butler, E. Clément, O. Dorvaux, S. Eeckhaudt, B. J. P. Gall, A. Görgen, T. Grahn, *et al.*, Phys. Rev. Lett. **98**, 132503 (2007).

[34] D. Peterson, B. B. Back, R. V. F. Janssens, T. L. Khoo, C. J. Lister, D. Seweryniak, I. Ahmad, M. P. Carpenter, C. N. Davids, A. A. Hecht, *et al.*, Phys. Rev. C **74**, 014316 (2006).

[35] Y. T. Oganessian, V. K. Utyonkov, Y. V. Lobanov, F. S. Abdullin, A. N. Polyakov, I. V. Shirokovsky, Y. S. Tsyganov, A. N. Mezentsev, S. Iliev, V. G. Subbotin, *et al.*, Phys. Rev. C **64**, 054606 (2001).

[36] H. Gäggeler, D. Jost, A. Türler, P. Armbruster, W. Brüchle, H. Folger, F. Heßberger, S. Hofmann, G. Münzenberg, V. Ninov, *et al.*, "Nucl. Phys. A **502**, 561 (1989).

[37] I. Dragojević, K. E. Gregorich, C. E. Düllmann, M. A. Garcia, J. M. Gates, S. L. Nelson, L. Stavsetra, R. Sudowe, and H. Nitsche, Phys. Rev. C **78**, 024605 (2008).

[38] G. Münzenberg, S. Hofmann, H. Folger, F. P. Heßberger, J. Keller, K. Poppensieker, B. Quint, W. Reisdorf, K. H. Schmidt, H. J. Schött, *et al.*, Z. Phys. A **322**, 227 (1985).

[39] G. Münzenberg, P. Armbruster, S. Hofmann, F. P. Heßberger, H. Folger, J. G. Keller, V. Ninov, K. Poppensieker, A. B. Quint, W. Reisdorf, *et al.*, Z. Phys. A **333**, 163 (1989).

[40] N. Sato, H. Haba, T. Ichikawa, D. Kaji, Y. Kudou, K. Morimoto, K. Morita, K. Ozeki, T. Sumita, A. Yoneda, *et al.*, J. Phys. Soc. Jpn. **80**, 094201 (2011).

[41] V. Weisskopf, Phys. Rev. **52**, 295 (1937).

[42] N. Bohr and J. A. Wheeler, Phys. Rev. **56**, 426 (1939).

[43] H. Lü, D. Boilley, Y. Abe, and C. Shen, Phys. Rev. C **94**, 034616 (2016).

[44] P. Möller, J. R. Nix, W. D. Myers, and W. J. Swiatecki, At. Data Nucl. Data Tables **59**, 185 (1995).

[45] W. D. Myers and W. J. Świątecki, Phys. Rev. C **60**, 014606 (1999).

[46] A. J. Pacheco, J. O. F. Niello, D. E. DiGregorio, M. di Tada, J. E. Testoni, Y. Chan, E. Chávez, S. Gazes, E. Plagnol, and R. G. Stokstad, Phys. Rev. C **45**, 2861 (1992).

[47] F. P. Heßberger, Eur. Phys. J. A **53**, 75 (2017).

[48] R. Capote, M. Herman, P. Obložinský, P. G. Young, S. Goriely, T. Belgya, A. V. Ignatyuk, A. J. Koning, S. Hilaire, V. A. Plujko, *et al.*, Nucl. Data Sheets **110**, 3107 (2009).

[49] M. Kowal, P. Jachimowicz, and A. Sobiczewski, Phys. Rev. C **82**, 014303 (2010).

[50] A. Baran, M. Kowal, P.-G. Reinhard, L. Robledo, A. Staszczak, and M. Warda, "Nucl. Phys. A **944**, 442 (2015), special Issue on Superheavy Elements.

[51] A. V. Ignatyuk, G. Smirenkin, and A. Tishin, Yad. Fiz. **21**, 485 (1975).

[52] H. Kramers, Physica **7**, 284 (1940).

[53] G. Henning, T. L. Khoo, A. Lopez-Martens, D. Seweryniak, M. Alcorta, M. Asai, B. B. Back, P. F. Bertone, D. Boilley, M. P. Carpenter, *et al.*, Phys. Rev. Lett. **113**, 262505 (2014).

[54] P. Möller, A. J. Sierk, T. Ichikawa, A. Iwamoto, and M. Mumpower, Phys. Rev. C **91**, 024310 (2015).

[55] P. Jachimowicz, M. Kowal, and J. Skalski, Phys. Rev. C **95**, 014303 (2017).

[56] P. Möller, A. J. Sierk, T. Ichikawa, and H. Sagawa, At. Data Nucl. Data Tables **109-110**, 1 (2016).

[57] H. Lü and D. Boilley, EPJ Web of Conferences **62**, 03002 (2013).